Magneto-Optic Kerr Effects in Gadolinium*

J. L. Erskine and E. A. Stern
Department of Physics, University of Washington, Seattle, Washington 98195
(Received 24 October 1972)

An investigation of magneto-optic effects in gadolinium metal is reported. Samples prepared by vacuum evaporation were studied *in situ* under ultra-high-vacuum conditions to ensure clean optical surfaces. Magneto-optic Kerr rotation and ellipticity, determined using a null-type ellipsometric method, are used to calculate the magnetic contribution to the conductivity tensor. Data cover the 1–5-eV range at several temperatures. A simple model based on band calculations is used as a basis for interpretation of the data. The magneto-optic absorption is shown to have an intraband component and an interband component in analogy with ordinary optical absorption. A phenomenological intraband theory of the magneto-optic Kerr effect is presented and used to subtract out the intraband contribution from experimental data. Structure observed in the interband magneto-optic contribution to the conductivity is discussed in terms of $p \rightarrow d$ and $d \rightarrow f$ transitions. Numerical estimates of the signs and weights of these transitions are made in order to support this interpretation. A number of experimentally determined parameters associated with the band structure of Gd result from this work including d bandwidth and general shape, location of unoccupied $4f$ states above the Fermi level, and the amount of "p character" in occupied bands. It is found that the unoccupied d bands have sharper structure and only qualitative agreement in the placement of the peaks compared to band calculations. The unoccupied $4f$ states are at a higher energy than predicted by calculations.

I. INTRODUCTION

The rare-earth metals form a unique series of elements characterized by the successive filling of their $4f$ shells with electrons. These partially filled $4f$ shells exhibit localized magnetic moments which are coupled in the solid by an exchange interaction involving conduction electrons. This coupling, in conjunction with the crystal field, produces a wide variety of magnetic ordering arrangements and results in unusual optical and transport-related behavior associated with magnetic ordering. The physical nature of these metals provides a unique opportunity for studying the details of exchange mechanisms, crystal-field effects, and optical behavior related to magnetic ordering.

An accurate band model for rare-earth metals is a necessary starting point for a detailed understanding of their magnetic and optical properties. The most detailed band models for rare-earth metals have resulted from band-structure calculations.[1] Properties of rare-earth metals have been studied by a number of standard experimental techniques in attempts to verify band-model predictions and improve these models. Optical experiments have revealed anomalies in the optical behavior of rare-earth metals related to magnetic ordering, but have been unable to provide detailed information on their band structure.[2] Recent photoemission results show evidence of having identified the $4f$ energy levels in a number of rare-earth metals, and other photoemission studies have provided some information about the conduction-band density of states.[3] Spin-polarized photoelectrons have been observed from the transition-metal ferromagnets as well as from gadolinium,[4] and these experiments provide information on electron spin as a function of energy in the bands. However, there has been some controversy over these results and predictions of the Stoner model, although the questions seem now to have been resolved.[5]

Ordinary optical experiments and photoemission experiments provide complementary information on the band structure of solids. Analogously, magneto-optic Kerr-effect studies and spin-polarized-photoemission studies represent complementary experimental techniques. Photoemission experiments have the advantage of selecting from all allowed optical transitions only those with a specific final energy represented by the energy distribution curves for emitted electrons. Disadvantages of photoemission experiments are interpretation of the data which is complicated by surface and scattering effects and also limitations on the energy range which can be covered owing to the work function.

Optical experiments provide less specific information than photoemission experiments since ordinary optical absorption is related to the sum of all allowed transitions at a specific energy. On the other hand, interpretation of optical data is basically more straightforward. Optical and magneto-optical studies are not restricted by work-function considerations and are less sensitive to the effects of surface potentials and scattering. Also, magneto-optic techniques have several important advantages over all other experimental methods for studying the electronic structure of

ferromagnets; the advantages will be discussed in this paper.

These observations provided part of the motivation for beginning a study of magneto-optic effects in rare-earth metals. Gadolinium was chosen as the first candidate since it has been most extensively studied using other experimental techniques, and its band structure has been calculated. Also, it has the highest Curie temperature and exhibits only a ferromagnetic ordered phase unlike the other rare earths, most of which exhibit a variety of magnetic ordering arrangements. The primary objective of the study was to obtain information on the band structure of gadolinium metal from its magneto-optic spectrum. To our knowledge there has been no previous work which has been able to ascertain quantitatively the main band-structure features from magneto-optic data. Cooper[6] attempted to use the low-frequency resonance in the magneto-optic spectra of Ni to choose between several different models of the band structure at the symmetry point L, and to obtain the exchange splitting, but no attempt was made to explain the main features of the spectra in terms of band structure.

The paper is organized as follows. Section II reviews the theory of magneto-optic Kerr effects and provides information needed for discussion in following sections. A useful sum rule is given which applies to off-diagonal elements of the conductivity tensor of magnetized and nonmagnetized solids. An intraband theory of magneto-optic Kerr effects is also presented in this section which accounts for the "conduction-electron" contribution to magneto-optic Kerr effects.

Section III discusses experimental techniques including sample preparation and ellipsometric methods used to measure magneto-optic Kerr rotation and ellipticity. Magneto-optic data, obtained using the techniques discussed, appear to have higher resolution than previous work on iron, nickel, and cobalt. Experimental results are presented in Sec. IV.

In Sec. V a band model is proposed for gadolinium metal. The model is based on the results of band calculations, on general theoretical arguments, and experimental information. In Sec. VI, this model is used to calculate the weights of structure in the magneto-optic spectrum of gadolinium, and the results are discussed in Sec. VII. Section VIII summarizes the results and conclusions of the study, pointing out areas of future interest.

II. MAGNETO-OPTIC KERR EFFECT

Plane-polarized light reflected from a magnetized ferromagnetic metal becomes elliptically polarized with its major axis slightly rotated from the original polarization direction. Components of the rotation and ellipticity which are linear functions of the sample magnetization are referred to as magneto-optic Kerr effects. Macroscopically, it is convenient to describe these effects by relating them to a conductivity tensor which characterizes the medium response to applied electromagnetic fields.

Using general symmetry arguments, it is easy to show that for a solid with cubic or greater symmetry, and magnetization $\vec{M}$ along the $\hat{z}$ direction, the conductivity tensor is of the form

$$\overleftrightarrow{\sigma}(\vec{M}) = \begin{pmatrix} \sigma_{xx} & \sigma_{xy} & 0 \\ -\sigma_{xy} & \sigma_{xx} & 0 \\ 0 & 0 & \sigma_{xx} \end{pmatrix} . \tag{1}$$

The ferromagnetic rare-earth metals all have hexagonal lattices, and therefore a more complicated tensor is required in the general case to correctly describe their magneto-optic behavior. However, Eq. (1) is suitable for polycrystalline gadolinium samples as will be justified in the following discussion. Ferromagnets exhibit off-diagonal terms σ_{xy} which are linear functions of the magnetization (to second order in $\vec{M}$) and represent the magneto-optic Kerr-effect contribution to $\overleftrightarrow{\sigma}$. Diagonal components of $\overleftrightarrow{\sigma}$ can exhibit only an even-power dependence on the magnetization as required by symmetry. Real and imaginary components of each element $\sigma_{ij} = \sigma_{ij}^{(1)} + i\sigma_{ij}^{(2)}$ also satisfy dispersion relations required by causality. The real component of diagonal elements, $\sigma_{xx}^{(1)}$, represents the absorptive part which describes ordinary optical absorption, and is always positive. The imaginary component of off-diagonal elements, $\sigma_{xy}^{(2)}$, represents the magneto-optic Kerr-effect absorptive part, and can be of either sign since it is proportional to the difference in absorption for left and right circularly polarized light. The dispersive parts of diagonal and off-diagonal elements of $\overleftrightarrow{\sigma}$ are $\sigma_{xx}^{(2)}$ and $\sigma_{xy}^{(1)}$, respectively. The difference in superscripts for absorptive parts of diagonal and off-diagonal components of $\overleftrightarrow{\sigma}$ are a result of using the convention[7] which does not multiply off-diagonal terms by the imaginary number $\sqrt{(-1)}$.

Spin-orbit interactions in the solid provide a means of coupling the magnetic dipole associated with electron spin to electric dipole transitions produced by incident light. This is the accepted physical basis of magneto-optic effects in ferromagnets.[8] Microscopic theories of magneto-optic Kerr effects have been discussed in detail elsewhere,[6,7] and this section serves only to present some additional work and provide background material for the discussion which follows.

In analogy with ordinary optical effects, it is appropriate to discuss microscopic origins of magneto-optic effects from an intraband or inter-

band viewpoint depending on the wavelength of light and characteristics of the metal under study. General expressions have been derived for the magnetic contribution to the conductivity of solids which take into account both spin-orbit effects and effects related to direct interaction of electrons with applied magnetic fields.[7]

The expression for the off-diagonal absorptive component of $\overleftrightarrow{\sigma}$ can be written as the sum of separate contributions from spin-up and spin-down electron states:

$$\sigma_{xy}^{(2)}(\omega)=\sigma_{xy\uparrow}^{(2)}(\omega)+\sigma_{xy\downarrow}^{(2)}(\omega)\ . \tag{2}$$

The contribution from spin-up states is given by[7]

$$\sigma_{xy\uparrow}^{(2)}(\omega)=\frac{\pi e^2}{4\hbar\omega m^2 V}\sum_{\alpha\beta}\{|\langle\beta\uparrow|\vec{\pi}^-|\uparrow\alpha\rangle|^2 - |\langle\beta\uparrow|\vec{\pi}^+|\uparrow\alpha\rangle|^2\}\delta(\omega_{\beta\alpha\uparrow}-\omega)\ , \tag{3}$$

where the operators $\vec{\pi}^{\pm}=\vec{\pi}_x\pm\vec{\pi}_y$ are linear combinations of the kinetic-momentum operator defined by $\vec{\pi}=\vec{p}+(\hbar/4mc^2)\vec{\sigma}\times\vec{\nabla}\ V(r)$, $\vec{p}$ being the canonical-momentum operator and the $\vec{\sigma}\times\vec{\nabla}V(r)$ term representing a spin-orbit contribution. In principle, the spin-orbit contribution to $\vec{\pi}$ could couple spin-up to spin-down states preventing a division of $\sigma_{xy}^{(2)}$ into separate spin-up and spin-down parts as in Eq. (2). However, this spin-flip contribution is second order in the spin-orbit interaction and is negligible compared to the contribution which conserves spin. Correct spin-up wave functions in Eq. (3) (Bloch states in the case of metals) are specified by $|\uparrow\alpha\rangle$, the occupied states, and $|\uparrow\beta\rangle$, the unoccupied states.[9] These states are normalized in the sample volume V. The expression for spin-down states is formally identical to Eq. (3) with spin-down states substituted for spin-up ones. Multiplying Eq. (3) by ω, adding the corresponding expression for $\sigma_{xy\downarrow}^{(2)}$, and expressing the sum over the states α and β in terms of an integral yield

$$\omega(\sigma_{xy\uparrow}^{(2)}(\omega)+\sigma_{xy\downarrow}^{(2)}(\omega)) = \omega\sigma_{xy}^{(2)}(\omega)=\frac{\pi e^2}{4\hbar m^2}\ \frac{1}{(2\pi)^3}\int F_{\alpha\beta}(\omega)\ \delta(\omega_{\beta\alpha}-\omega)d^3k\ , \tag{4}$$

where

$$F_{\alpha\beta}(\omega)=|\langle\beta\uparrow|\vec{\pi}^-|\uparrow\alpha\rangle|^2-|\langle\beta\uparrow|\vec{\pi}^+|\uparrow\alpha\rangle|^2 + |\langle\beta\downarrow|\vec{\pi}^-|\downarrow\alpha\rangle|^2-|\langle\beta\downarrow|\vec{\pi}^+|\downarrow\alpha\rangle|^2.$$

If we define an average matrix element $\overline{F}_{\alpha\beta}$ by

$$\int F_{\alpha\beta}(\omega)\,\delta(\omega_{\beta\alpha}-\omega)d^3k=\overline{F}_{\alpha\beta}(\omega)\int\delta(\omega_{\beta\alpha}-\omega)d^3k\ , \tag{5}$$

then Eq. (4) can be written as

$$\omega\sigma_{xy}^{(2)}(\omega)=\frac{\pi e^2}{4\hbar m^2}\ \overline{F}_{\alpha\beta}(\omega)J_{\alpha\beta}(\omega)\ , \tag{6}$$

where $J_{\alpha\beta}(\omega)$ is the familiar joint-density-of-states function

$$J_{\alpha\beta}(\omega)=\frac{1}{(2\pi)^3}\int\delta(\omega_{\beta\alpha}-\omega)d^3k\ . \tag{7}$$

If we assume that $\overline{F}_{\alpha\beta}(\omega)$ is a constant independent of ω, then the quantity $\omega\sigma_{xy}^{(2)}(\omega)$ is directly proportional to the joint density of states in the solid. Further on in the paper we discuss when the approximate constancy of $\overline{F}_{\alpha\beta}(\omega)$ is justified.

Optical and magneto-optical spectra of metals contain contributions from both intraband and interband effects. Accounting for intraband contributions to the total observed optical or magneto-optical absorption of a metal is a helpful first step in understanding the origin of structure in these spectra. In principle, Eq. (3) accounts for both interband and intraband effects; however, there is a more practical framework for discussing intraband effects. The remainder of this section summarizes a phenomenological theory of intraband magneto-optic effects.

In discussing the Karplus–Luttinger[10] treatment of anomalous Hall effects in ferromagnets, Smit[11] pointed out that spin-orbit interactions cause an electron with wave vector $\vec{k}$ to have associated with it a dipole moment $\vec{P}(\vec{k})$ per unit cell. When external electric fields are applied, the distribution function $f(\vec{k})$, which gives the probability that a state $\vec{k}$ is occupied, is changed resulting in a distortion of charge density in a unit cell and a net macroscopic dipole moment $\vec{P}_0$ given by

$$\vec{P}_0=\int f(\vec{k})\vec{P}(\vec{k})d^3k\ . \tag{8}$$

According to Smit, $\vec{P}_0$ is proportional to the magnetization and normal to it, and proportional to the primary current and normal to it. Assuming $\vec{P}(\vec{k})$ also satisfies these requirements, it can be simply characterized *on a spherical Fermi surface* by

$$\vec{P}(\vec{k})=A\vec{k}\times\vec{M}\ , \tag{9}$$

where $\vec{M}$ is the magnetization, $\vec{k}$ is the electron wave vector, and A is a constant. The magnitude of $\vec{P}(\vec{k})$ is determined by the strength of spin-orbit coupling, contained in A, while the distortion of $f(\vec{k})$ from equilibrium, and hence $\vec{P}_0$, is moderated by normal scattering processes.

Spin-orbit and exchange interactions affect the conductivity of a solid in several ways. At low frequencies, spin-orbit effects on scattering processes dominate and result in anomalous Hall effects as discussed by Fivaz[12] and Berger.[13] At optical frequencies, the macroscopic dipole moment $\vec{P}_0$ will oscillate with the distribution function, which is driven by applied fields, producing a polarization current.[14] The total current can be written

$$\vec{J} = \vec{J}_{\text{cond}} + \vec{J}_{\text{pol}} = e\int \vec{v}(\vec{k}) f(\vec{k}) d^3k + \frac{d\vec{P}_0}{dt} , \qquad (10)$$

where $\vec{v}(\vec{k}) = (1/\hbar)\vec{\nabla}_k[E(\vec{k}) - \vec{P}(\vec{k})\cdot\vec{\epsilon}]$, $E(\vec{k})$ are the Bloch energies, and $\vec{\epsilon}$ is the electric field which modifies the Bloch energies through the classical interaction with the dipole moment $\vec{P}(\vec{k})$.

The current, given by Eq. (10), is now evaluated taking into account spin-orbit and exchange effects at all frequencies. The method outlined in the following is different from previous treatments of the problem but has the advantage of separating effects due to scattering from effects due to applied electric fields. This is important because there is a controversy in the literature[13] which is concerned with the validity of the so-called "dipole driving mechanism" which occurs because of the simultaneous presence of scattering, the electric field, and spin-orbit effects. Our approach[15] permits us to sidestep any *ad hoc* assumptions about this term, and to eliminate this uncertainty from the calculation.

Consider an electric field of the form

$$\vec{\epsilon}(t) = \epsilon_0 \delta(t)\hat{x} \qquad (11)$$

applied to a ferromagnetic metal. There is no scattering during the application of $\vec{\epsilon}(t)$ which occurs in an infinitesimal time, and the total effect is to shift each $\vec{k}$ state from its initial value $\vec{k}_0$ to a new value

$$\vec{k} = \vec{k}_0 + \vec{\Delta} , \qquad (12)$$

where

$$\vec{\Delta} = (e\epsilon_0/\hbar)\hat{x} , \qquad (13)$$

and $\hat{x}$ is a unit vector in the x direction. This shift of $\vec{k}$ states at $t = 0^+$ is shown in Fig. 1 where a spherical Fermi surface has been assumed for simplicity.

For $t > 0$, there are no driving fields present, and assuming the relaxation-time approximation, each $\vec{k}$ state relaxes back to its original value according to

$$-\frac{d\vec{k}}{dt} = \frac{\vec{k}}{\tau} + \frac{\vec{s}\times\vec{k}}{\tau_s} , \qquad (14)$$

where the right-hand side of Eq. (14) contains a normal scattering lifetime characterized by τ, and a skew scattering lifetime characterized by τ_s which accounts for the spin-orbit asymmetric scattering in ferromagnetic metals.[12] The total current for $\tau > 0$ is obtained by integrating the contribution from $\vec{k}$ states in the electron and hole slices of $\vec{k}$ space shown in Fig. 1. Choosing $\hat{s}$ along the z direction and solving for the y component of current yields

$$\frac{J_y(t)}{\epsilon_0} = \frac{ne^2}{m^*} e^{-t/\tau}\sin\Omega t$$

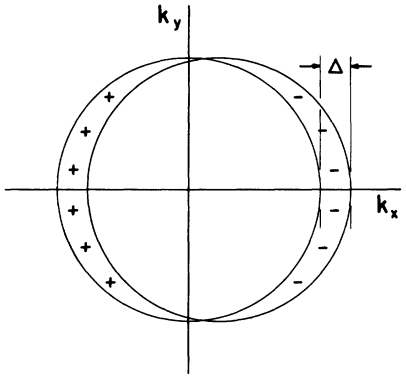

FIG. 1. Displacement of $\vec{k}$ states resulting from application of a δ-function electric field $\epsilon = \epsilon_0\delta(t)\hat{x}$, $\Delta = (e/\hbar)\epsilon_0$. Electron excitations are in the right crescent (–) while hole excitations are in the left crescent (+).

$$+\frac{d}{dt}\frac{\Delta n e|P_0'|}{m^* v_0} e^{-t/\tau}\cos\Omega t , \qquad (15)$$

where $\Omega = s/\tau_s$, $s = \pm 1$ for spin-up and spin-down states, v_0 is the Fermi velocity, $|P_0'|$ is the maximum value of $\vec{P}(\vec{k})$, m^* is the effective mass of conduction electrons, and $\Delta n = n_\uparrow - n_\downarrow$ is the difference in the number of spin-up and spin-down electrons per unit volume.

The conductivity as a function of frequency is obtained by Fourier analysis:

$$\sigma_{xy}(\omega) = \int_0^\infty \frac{J_y(t)}{\epsilon_0} e^{-i\omega t} dt , \qquad (16)$$

which by elementary integration yields

$$\sigma_{xy}(\omega) = \frac{\omega_p^2}{4\pi}\frac{\Omega}{\Omega^2 + (1/\tau + i\omega)^2} - \frac{\omega_p^2}{4\pi}\langle\sigma_z\rangle \times\frac{|P_0'|}{ev_0}\left(1 - \frac{i\omega(1/\tau + i\omega)}{\Omega^2 + (1/\tau + i\omega)^2}\right) , \qquad (17)$$

where $\omega_p^2 = 4\pi ne^2/m^*$, and $\langle\sigma_z\rangle = (n_\uparrow - n_\downarrow)/(n_\uparrow + n_\downarrow) = \Delta n/n$ describes the fractional spin polarization. It is straightforward to show that there is no contribution to $J(t)$ which results during application of $\vec{\epsilon}(t)$.

In the high-frequency limit, defined by $\omega\tau \gg 1$, $\omega\tau_s \gg 1$, Eq. (17) reduces to

$$\sigma_{xy}^{(1)}(\omega) = \frac{-\omega_p^2}{4\pi}\langle\sigma_z\rangle\frac{|P_0'|}{ev_0}\frac{1}{(\omega\tau)^2} , \qquad (18)$$

$$\sigma_{xy}^{(2)}(\omega) = \frac{\omega_p^2}{4\pi}\langle\sigma_z\rangle\frac{|P_0'|}{ev_0}\frac{1}{(\omega\tau)} , \qquad (19)$$

which are the appropriate expressions valid at the optical frequencies of interest in this paper. In the limit $\omega \to 0$, Eq. (17) reduces to the result obtained by Fivaz provided $\Omega^2 \ll 1/\tau^2$. The discrepancy is due to the "dipole-driving" term included

in Fivaz's calculation[12] which does not enter into the treatment presented here. The high-frequency limit, Eq. (19), agrees with an expression derived by Doniach.[16] Eliminating the dipole-driving-term contribution from expressions derived by Fivaz and by Doniach brings their results into agreement with our results at $\omega = 0$ and with the results of Berger.[13]

We conclude this section by presenting a sum rule for the off-diagonal elements of $\vec{\sigma}$. A similar result has been given previously,[7] which applies to nonferromagnetic metals. Accounting for both the applied magnetic field and net spin polarization, the sum rule becomes

$$\int_0^\infty \omega\sigma_{xy}^{(2)}(\omega) = \frac{\pi e^2\hbar}{8m^3c^2V}\sum_\alpha \langle\alpha|\sigma_z\nabla^2 V(r)|\alpha\rangle + \frac{\pi e^3}{2m^2c}\vec{H}_z\bar{n} \,. \quad (20)$$

In Eq. (20), σ_z is the spin operator, $V(r)$ is the potential, $\vec{H}_z$ is the magnetic field assumed along the $\hat{z}$ direction, and $\bar{n} = N/V$ is the number of atoms per unit volume. The sum is over all occupied states which contribute a net spin polarization to the solid.

III. EXPERIMENTAL TECHNIQUES

Samples were prepared by vacuum evaporating 1-g charges of 99.9%-pure gadolinium from tantalum boats onto glass or sapphire substrates. Pressures in the all-metal Vac-Ion-pumped vacuum system, just after an evaporation, were typically in the low-10^{-10}-Torr range. Samples were studied *in situ* at these pressures to ensure clean optical surfaces. Data taken on successive days using the same sample showed no appreciable variation. After all optical data had been taken, samples were removed from the vacuum chamber and x-ray analysis was used to determine crystal structure and check for bulk impurities.

Substrate temperatures, evaporation rates, film thickness, and pressure during evaporation were found to influence crystal structure of the prepared films. Thicker films (5000 Å) prepared on substrates held at temperatures above 300 °C, and using evaporation rates below 10 Å/sec, were found to exhibit a high degree of preferred orientation, with the c-axis direction normal to the substrate. Films prepared at lower substrate temperatures, and at higher evaporation rates tended to consist of more randomly oriented crystallites.

The sample holder, mounted at the tip of a helium Dewar, provided temperatures down to 10 °K. The possibility of strain effects changing measured properties of thin films, owing to differences in thermal expansion coefficients of the film and substrate, has been considered previously by Schüler.[3] This study verified that the dependence of electrical resistivity on temperature for bulk and thin-film gadolinium samples is nearly identical aside from a slightly higher residual resistance of the films, presumably due to differences in crystallite size. Evidence that magneto-optic effects observed using the thin films are also characteristic of bulk-sample magneto-optic properties is presented later in this paper.

Magneto-optic Kerr rotation and ellipticity were measured using a null-type ellipsometric technique.[17] Collimated monochromatic plane-polarized light provided by a 1000-W arc lamp, $\frac{1}{4}$-m grating monochromator, off-axis mirror, and polarizing prism is incident at a 30° angle of incidence as shown in Fig. 2. Reflected light is, in general, elliptically polarized, and can be characterized at a specific wavelength, temperature, and angle of incidence by a complex number, $\phi = \theta + i\epsilon$, where θ is the rotation of the ellipse major axis from the original plane of polarization and ϵ is the ellipticity of the ellipse. The sample is magnetized in the plane of incidence as shown in Fig. 2, and a portion of ϕ is a linear function of the magnetization, $\phi'(M) = \theta'(M) + i\epsilon'(M)$. The components $\theta'(M)$ and $\epsilon'(M)$ are referred to as the magneto-optic Kerr rotation and ellipticity, respectively. The magnetic contribution $\phi'(M)$ is easily separated from the total ϕ by reversing the magnetic field. Rotation and ellipticity can be determined as follows: With the sample magnetized in a particular direction, the analyzing prism (see Fig. 2) is adjusted to yield a minimum of transmitted light. When $\vec{M}$ is reversed, the analyzing prism must be rotated by an amount $2\theta'$ to restore minimum intensity. By introducing a $\frac{1}{4}$-wave phase shift, the imaginary component $2\epsilon'$ is determined in the same

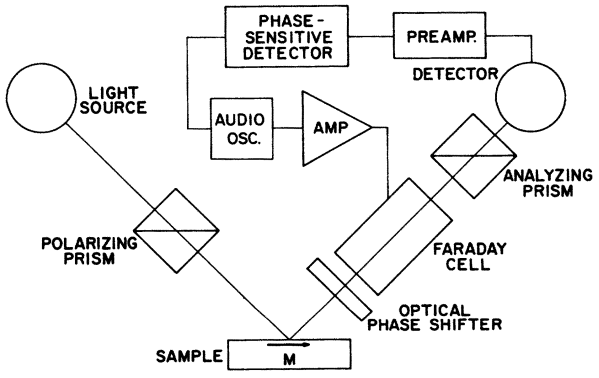

FIG. 2. Null-type ellipsometer block diagram. Samples were vacuum evaporated and maintained in the ultra-high vacuum at the tip of a helium Dewar (not shown). A large electromagnet (not shown) provided fields to 2000 Oe to saturate the sample magnetization in the plane of incidence and parallel to its surface.

manner.

In order to optimize the sensitivity of this method it is necessary to introduce a light modulator and use phase-sensitive detection techniques. Our modulator operated at 1 kHz, and consisted of a water-cooled solenoid surrounding a transparent core material with a high Verdet constant. All cores used were carefully checked for strain or other birefringence. Best results for visible and infrared wavelengths were obtained using Schott SF-6 glass rods. In the ultraviolet range, silica rods and quartz dye cells filled with distilled water were found suitable. Detected intensity of light is given by

$$I(t) = I_0 + I_1 \sin^2(\theta + \alpha \sin\omega_0 t)$$
$$\approx I_0 + I_1(\theta + \alpha \sin\omega_0 t)^2 , \qquad (21)$$

where I_0/I_1 defines the extinction ratio of the optical system, θ measures the deviation of the major axis of polarization from the extinction condition, and α is the modulation amplitude. At a null, defined by $\theta = 0$, the ω_0 component of detected intensity vanishes, which can be precisely monitored using phase-sensitive detection techniques.

Typical values of magneto-optic rotation and ellipticity observed in gadolinium samples at 105 °K were 3 minutes of arc. Near room temperature, values were considerably smaller. In order to achieve 1% accuracy, an angular resolution of about 2 arc seconds is required. This resolution was achieved at a signal-to-noise ratio of 10 over most of the 1–5-eV energy range covered using a spectral resolution $\Delta\lambda/\lambda$ of 1% and a 10-sec phase-detector integration time constant.

Rather than measure magneto-optic Kerr rotation and ellipticity directly by mechanically adjusting the analyzing prisms a second coil was added to the Faraday cell enabling magneto-optic rotations to be precisely cancelled by a stable dc. This method has the advantage of minimizing the effects of mechanical disturbances of the optical bench during a measurement. Accurate calibration of the system was obtained by rotating the analyzing prism through a relatively large angle (3°) from null and measuring the dc needed to restore the null condition.

Rotations were measured by saturating the ferromagnetic sample in one direction, establishing a null, reversing the field, and recording the current needed to cancel $2\theta'$, twice the magneto-optic Kerr rotation. Ellipticities were measured in a similar manner by introducing a $\frac{1}{4}$-wave phase shift before the Faraday-cell modulator.

The electromagnet used to saturate films produced fringe fields which caused significant rotations in vacuum windows, prisms, the phase shifter, and the Faraday cell. These "zero-correction" errors were accounted for at each wavelength by replacing the ferromagnetic sample with a silver sample. Reflection Faraday rotations of silver have been accurately determined[18] and are extremely small (less than one second of arc for magnetic fields used, $B \approx 2000$ Oe). Therefore when the silver sample was in place, the total rotation was essentially a zero correction.

Additional details of the ellipsometer, including specific components used and methods of optimizing sensitivity, and more information concerning the high-vacuum Dewar and other experimental apparatus, are available in Ref. 19.

IV. EXPERIMENTAL RESULTS

As a valuable initial check of the ellipsometer, magneto-optic Kerr effects of evaporated nickel films were studied before investigating rare earths. Magneto-optic data of nickel films at low temperatures were found to be in good agreement with results obtained using bulk samples. This agreement was taken as adequate evidence that magneto-optic data of thin-film samples are characteristic also of bulk magneto-optic properties. This agreement was additional evidence that strain effects in the films are not important in determining structure of magneto-optic Kerr-effect data.

Repeatability of magneto-optic Kerr-effect data for all gadolinium samples was found to be very good, and the fine-structure variations which were observed correlated with differences in crystal structure of the individual samples. For a given polarization direction, all gadolinium samples exhibited the same gross features in magneto-optic data independent of crystal structure. Gadolinium samples with a high degree of crystallite orientation exhibited some structural dependence in magneto-optic data related to initial polarization direction of incident light; other samples with randomly oriented crystallites showed much weaker polarization dependence. Nickel samples showed no observable polarization dependence. Polarization dependence of the unoriented gadolinium samples was small enough to justify using isotropic formulas[20] to calculate the off-diagonal conductivity, and the form of $\overleftrightarrow{\sigma}$ given by Eq. (1).

Optical constants used in calculating the off-diagonal conductivity from magneto-optic Kerr-rotation and ellipticity measurements are shown in Fig. 3. These results are basically those obtained by Hodgson[21]; slight modifications of his data were made in order to obtain better agreement with optical-constant measurements taken on samples used in this study.[22] Kramers–Krönig analysis was used to ensure that the resulting optical constants were consistent with causality requirements. Structure appearing in these data below 1 eV is clear evidence that interband effects

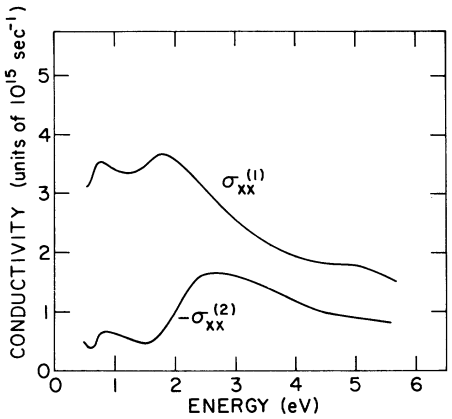

FIG. 3. Optical conductivity of Gd at 105 °K; $\sigma_{xx}^{(1)}$ absorptive part, $\sigma_{xx}^{(2)}$ dispersive part. The optical conductivity is related to optical constants $\epsilon_1(\omega)$ and $\epsilon_2(\omega)$ by $\sigma_{xx}^{(1)} + i\sigma_{xx}^{(2)} = \frac{1}{4}(\omega/\pi)(\epsilon_1 - 1 - i\epsilon_2)$.

are important in this energy range.

Figure 4 shows the magneto-optic Kerr rotation and ellipticity of polycrystalline gadolinium samples at 105 °K as a function of energy. These data actually represent an average of nearly identical results obtained from three different samples. X-ray analysis showed these three samples to be similar, consisting mainly of randomly oriented crystallites. The off-diagonal conductivity, shown in Fig. 5, was calculated using expressions for an isotropic solid.[20] Kramers–Krönig analysis of real and imaginary parts of σ_{xy} verified that their dispersion is consistent with causality conditions.

The increased sensitivity of the magneto-optic Kerr effect can be seen by comparing absorptive components of diagonal ($\sigma_{xx}^{(1)}$) and off-diagonal ($\sigma_{xy}^{(2)}$) elements of $\vec{\sigma}$. Off-diagonal components, which represent the magnetic contribution to $\vec{\sigma}$, exhibit more pronounced structure in the 1–5-eV range. Both normal and magnetic components of $\vec{\sigma}$ show a well-defined peak at 1.8 eV; however the peak in $\sigma_{xy}^{(2)}$ at 4.2 eV is not easily seen in $\sigma_{xx}^{(1)}$. It appears as though there may be a very broad peak in $\sigma_{xx}^{(1)}$ around 5 eV.

A number of samples were found to consist largely of oriented crystallites with their c axis normal to the substrate. From an optical point of view, these samples should behave as single crystals. Magneto-optical spectra of these samples differed in fine structure details from those of samples consisting of unoriented crystallites.[23] Differences were verified by measurements at several temperatures on a number of samples with ordered and unordered crystallite orientation.

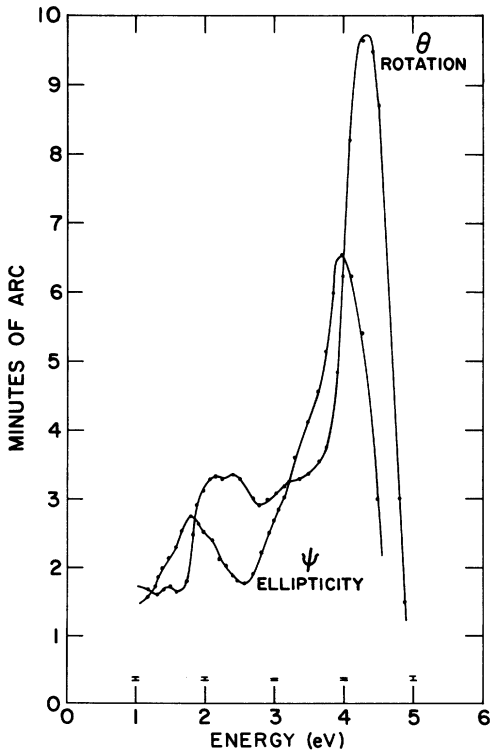

FIG. 4. Magneto-optic Kerr rotation and ellipticity of Gd at 105 °K. Curves represent an average of nearly identical data for three polycrystalline samples.

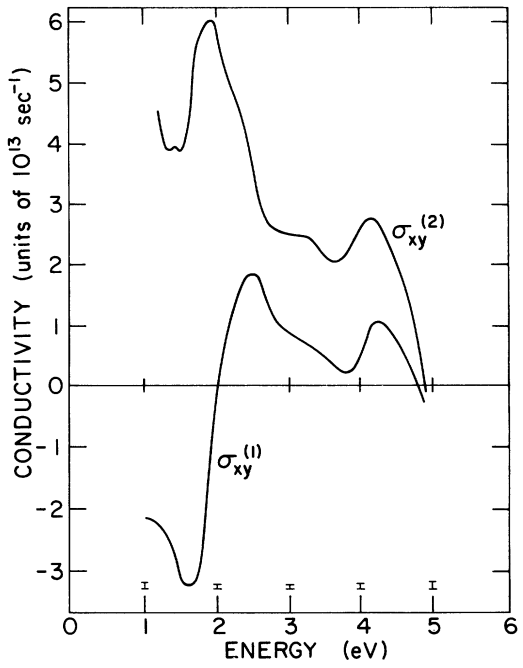

FIG. 5. Magnetic contribution to the optical conductivity of Gd at 105 °K; $\sigma_{xy}^{(2)}$ absorptive part, $\sigma_{xy}^{(1)}$ dispersive part. The relative errors at a given energy are shown by the bars at the bottom of the graph. The absolute values may have addition errors mainly due to the inaccuracies in the ordinary optical constants.

Typical results are shown in Figs. 6 and 7. Figure 6 shows magneto-optic Kerr rotation of an unordered crystallite sample at three temperatures, and an ordered crystallite sample at two temperatures. Inspection of the results indicates that characteristic structure of each is preserved at the different temperatures. Figure 7 shows the polarization dependence observed in an ordered crystallite gadolinium sample. Samples with randomly oriented crystallites showed much weaker polarization dependence.

V. BAND MODEL FOR GADOLINIUM

Our discussion of the magneto-optic data is based on a simplified band model which is now presented. We have used published band calculations for Gd as a guide in constructing our model as well as our experimental results which supplement the band calculations. Consider first atomic gadolinium which has a valence configuration of $4f^7 5d^1 6s^2$. The $4f$ shell, even though only partially filled, is more tightly bound than the filled $5s$ and $5p$ shells as shown in Fig. 8. In the solid, the $5d$ and $6s$ electrons of adjacent atoms overlap strongly, as indicated by the location of the Wigner–Seitz radius (Fig. 8), and are therefore broadened into bands. The $4f$ electrons overlap very little and are also only weakly affected by crystal-field effects due to shielding from the $5s$ and $5p$ states, and therefore preserve their atomic character.

Figure 9 shows the calculated bands of gadolinium at a number of symmetry points in the Brillouin zone. The lower-lying states are seen to be predominately s character and the relatively flat nature of bands near the Fermi level are characteristic of d states. A density-of-states histogram is shown in Fig. 10. The total area under this curve corresponds very nearly to 12 electrons, accounting for the ten $5d$ and two $6s$ atomic levels

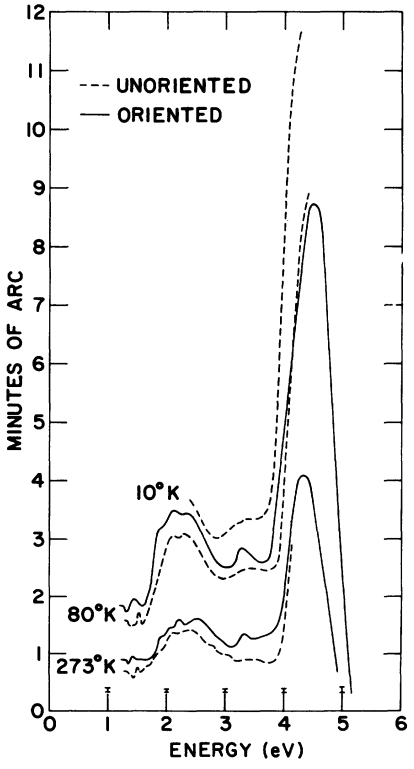

FIG. 6. Comparison between the magneto-optic Kerr rotation of oriented and unoriented (polycrystalline) Gd samples. The crystallite c axes of oriented samples were primarily normal to the optical surface. The fine structure is real as can be seen by comparing with the error bars at the bottom of the graph.

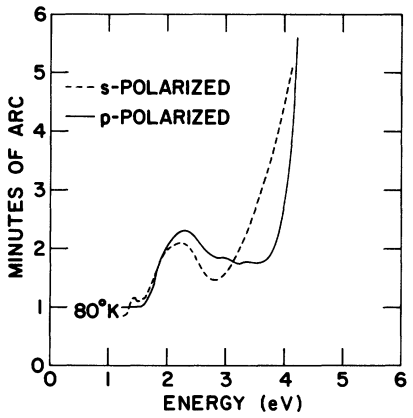

FIG. 7. Gross polarization dependence of magneto-optic Kerr rotation for oriented Gd samples as defined in caption for Fig. 6. The fine structure as shown in Fig. 6 has been smoothed over to focus on only the gross differences.

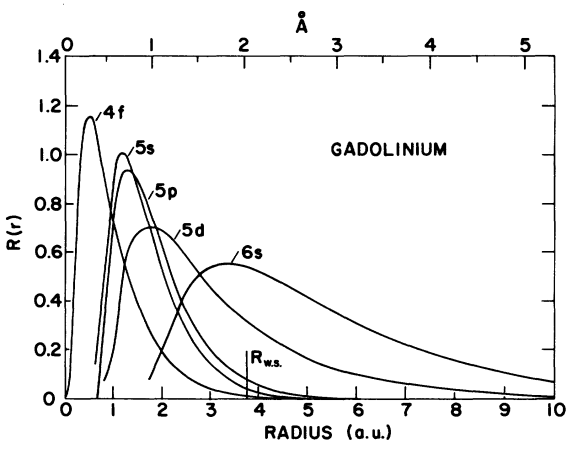

FIG. 8. Normalized radial wave function $R(r)$ for atomic Gd, where $\int[R(r)]^2 dr = 1$, after Herman and Skillman (Ref. 26). The oscillations for small r are not shown.

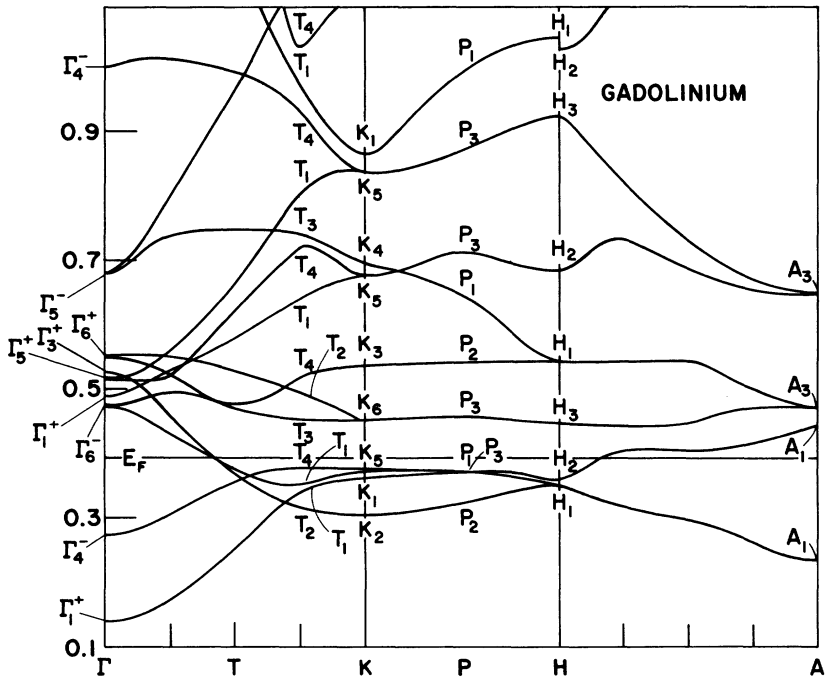

FIG. 9. Band structure of Gd metal [Dimmock *et al.* (Ref. 1)]. Note the flatness of the *d* bands.

and indicating that other states are not mixed into any great extent. The small amount of "*p* character" which exists in the occupied conduction-band states is expected to be concentrated in a region just below the Fermi level. The band-structure results suggest that occupied conduction-band states are predominately *d* character and that the *d* bands are split into two major groups. Splitting of *d* bands into two major subbands as suggested here has been observed in the tight-binding band calculations for transition-metal ferromagnets.[24] This effect, referred to as covalency splitting, has been discussed by Friedel and others.[25]

Our simplified band model is summarized by Fig. 11. Atomic energies are those given by Herman and Skillman[26]; band energies and widths

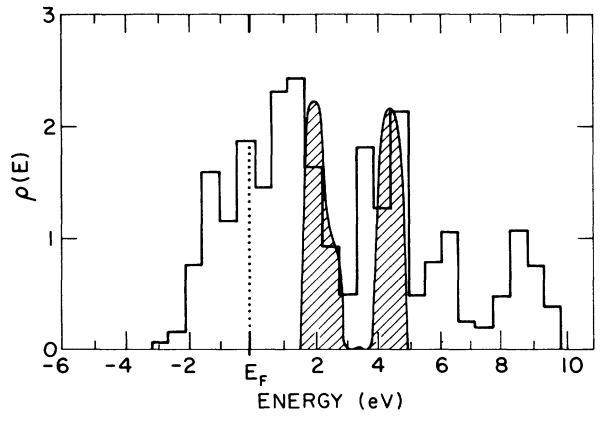

FIG. 10. Density of states of Gd metal. Histogram is as calculated by Dimmock *et al.* (Ref. 1) and hatched curve is the approximate density of states as determined experimentally by the magneto-optic Kerr effect. Experimental result covers only the range shown.

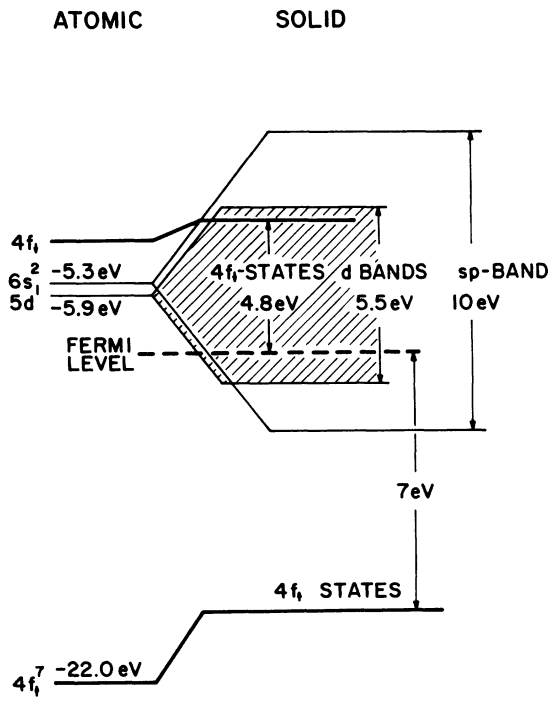

FIG. 11. Simplified model for Gd used to estimate the weights of the various transitions that contribute to $\langle \sigma_{xy}^{(2)} \rangle$.

are shown which agree with the data to be discussed in Sec. VI. Location of the occupied $4f$ level was chosen at -7 eV as suggested by photoemission results[27] and the work of Herbst *et al.*[28] The location of unfilled $4f$ levels in Gd metal according to theoretical work of Herbst *et al.*[28] is about 3.6 eV above the Fermi level. We will present arguments in Sec. VI which indicate that transitions from d states to unfilled $4f$ states are observed in our magneto-optic data. In the band model, Fig. 11, we have therefore used our experimentally determined location of the $4f$, levels. In the model, we choose the relative position of d bands, sp bands, and the Fermi band to yield one sp and two d states below the Fermi level in accordance with band-structure-calculation predictions.

VI. CALCULATIONS

As a first step in understanding the experimental data shown in Fig. 5, we evaluate the intraband contribution to $\sigma_{xy}^{(2)}(\omega)$ using Eq. (16). It is clear from Fig. 8 that atomic $5d$ electrons penetrate deeper into the core than the $6s$ electrons, and that they overlap more with polarized $4f$-electron states. Therefore, in the solid, we expect the "d-conduction" electrons to carry most of the conduction-electron contribution to the magnetic moment per atom, and exhibit stronger spin-orbit effects. We estimate spin-orbit effects of d-conduction electrons to be a factor of 50 larger than for p-character-conduction-band states. Intraband magneto-optic effects, being proportional to spin-orbit coupling and net spin polarization, will therefore be primarily due to the d character of conduction electrons.

To estimate the spatial polarization ($|P_0'|/e$), we equate the energy associated with a dipole $|P_0'|$ of charge e separated by distance a to the appropriate spin-orbit energy. The electrostatic dipole energy is $P_0'^2/a^3$ and by the Virial theorem the total dipole energy increase is $P_0'^2/2a^3$. This is driven by the spin-orbit energy estimated by $\xi_d\langle l\rangle$, where $\xi_d = 0.123\times10^{-12}$ ergs (0.077 eV) for $5d$ electrons in Gd,[26] and $\langle l\rangle$ is a characteristic angular momentum associated with a Fermi-level d state. The conduction d-electron density in Gd is $n_d = 0.611\times10^{23}$ cm^{-3} (assuming two d electrons per atom), and since in Gd the Fermi level is near the bottom of the d band, we can approximate by using a free-electron model to obtain $k_0 = (\frac{3}{2}\pi^2 n_d)^{1/3} = 9.7\times10^7$ cm^{-1}. To obtain k_0 we use the result of band calculations that two d bands contribute to the occupied states. In the solid, we estimate the average radial extent of d electrons in the Wigner–Seitz sphere to be $\frac{1}{2}a = 1.2$ Å (from Fig. 8). An estimate of $\langle l\rangle$ is given by $\frac{1}{2}k_0 a$. From these estimates, we find that

$$(|P_0'|/e) \approx (a^2/e)(\xi k_0)^{1/2} = 0.4 \text{ Å}.$$

The other parameters required to evaluate the intraband term [Eq. (16)] are chosen as follows: For the value of $\langle\sigma_z\rangle_d$ which characterizes the spin polarization, we choose a value of 0.28 to account for the 0.55 μ_B/atom contributed by the two d conduction electrons per atom in Gd. For the carrier lifetime τ, we use the result obtained by Hodgson[21] from optical data, $\hbar/\tau = 0.5$ eV. These values yield an intraband contribution of

$$\sigma_{xy}^{(2)}(\omega) = (8.0\times10^{13}/\hbar\omega)\,\text{sec}^{-1}, \tag{22}$$

where $\hbar\omega$ is in units of eV.

This result accounts for the general ω^{-1} behavior of $\sigma_{xy}^{(2)}(\omega)$ shown in Fig. 5. What remains after subtracting Eq. (22) from the experimental data is the interband contribution. This is observed to be a pair of peaks at 2 and 4.2 eV with a total weight for $\int\sigma_{xy}^{(2)}(\omega)\,d\omega$ of 2.0×10^{28} sec^{-2}. The division between interband and intraband contributions is most conveniently plotted as $\omega\sigma_{xy}^{(2)}$ vs ω, where the intraband term is a horizontal line as shown in Fig. 12.

Interband magneto-optic Kerr effects are governed by quantum-number selection rules $\Delta l = \pm1$, $\Delta m_l = \pm1$, and $\Delta s_z = 0$, corresponding to orbital momentum, Z component of orbital momentum, and spin, respectively. In the model of Sec. V, magneto-optical interband transitions are allowed from partially filled $4f$ levels and occupied p-character conduction-band states to d states

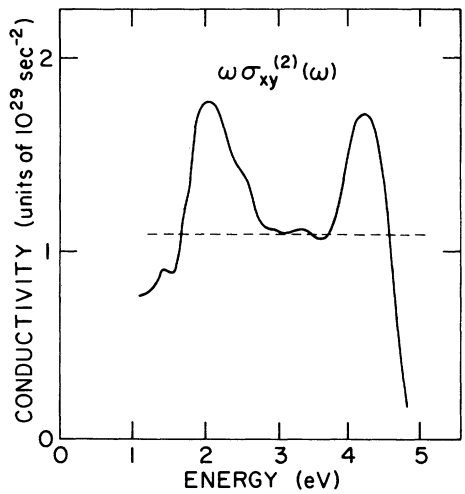

FIG. 12. Experimental values of $\omega\sigma_{xy}^{(2)}(\omega)$ at 105 °K as a function of energy. Area under the dotted line is the estimated intraband contribution; area above the dotted line is the estimated interband contribution mainly due to $p \rightarrow d$ transitions. The curve above the dotted line is the approximate d-state contribution to the density of states, also plotted in Fig. 10.

above E_F, and also from occupied d states to f- and p-character states above E_F. Interband magneto-optic absorption from these transitions is proportional to the joint density of occupied and unoccupied states. Preliminary motivation for interpretation of the interband part of $\sigma_{xy}^{(2)}(\omega)$ comes from examining the joint density-of-states function for p-character states below E_F and d states above E_F, which can be expressed

$$J_{(sp)d} = \int_{\omega_F}^{\omega_F-\omega} \rho_d(\nu)\,\rho_p(\nu+\omega)\,d\nu \ . \qquad (23)$$

A similar expression symbolized by $J_{(d)sp}$ can be written for occupied d states and empty p states. From our previous discussion of the nature of occupied p states, and reference to the density-of-states histogram, Fig. 10, it is evident that Eq. (23) gives a double-peak behavior similar to the behavior of the interband contribution of $\omega\sigma_{xy}^{(2)}(\omega)$, shown in Fig. 12. The function $J_{d(sp)}$ yields a broad structure with no sharp peaks. Therefore, our interpretation of the two peaks in the interband part of $\sigma_{xy}^{(2)}(\omega)$ is that they result from transitions between p-character states just below E_F to d bands above E_F. In the remainder of this section, we present additional evidence to support this interpretation of the structure in $\sigma_{xy}^{(2)}(\omega)$.

We now estimate the total magneto-optic absorption for each type of interband transition allowed by the model under consideration, and show that the estimated total weight $\langle\sigma_{xy}^{(2)}\rangle = \int\sigma_{xy}^{(2)}(\omega)\,d\omega$ contributed by $p \rightarrow d$ transitions is consistent with the predictions of band calculations and with experimental results. We also find that $d \rightarrow p$ transitions yield a contribution which is small compared to $p \rightarrow d$ transitions in the energy range of interest. The values of $\langle\sigma_{xy}^{(2)}\rangle$ for $f \rightarrow d$ and $d \rightarrow f$ transitions are also estimated.

Referring to Eq. (3), it is apparent that there are three distinct mechanisms which will yield interband magneto-optic Kerr effects. In one mechanism, spin-orbit coupling perturbs the ground-state wave functions $|\alpha\rangle$ and $|\beta\rangle$ and the off-diagonal conductivity is proportional to the spin-orbit perturbation parameter $\xi_{so}/\Delta E$, where ΔE is an interband energy. A second mechanism occurs when spin-orbit effects contribute directly to the current ($\vec{\pi}$ vector), and a third mechanism involves spin-orbit splitting of degenerate levels. In order to estimate the total weight of $\sigma_{xy}^{(2)}$ for $p \rightarrow d$, $d \rightarrow p$, $f \rightarrow d$, and $d \rightarrow f$ interband transitions, we consider an atomic model for gadolinium with spin-polarized d and f electrons giving 7.55 μ_B/atom. The question naturally arises whether an atomic calculation has any relationship to the solid where clearly band-broadening effects are stronger than the appropriate atomic splittings. We argue that such a calculation is justified based on the discussion in the next paragraph. It is straightforward to show by direct calculation that when spin-orbit coupling is added to the atomic model, only the third mechanism, just described, provides a nonzero first-order spin-orbit contribution to $\langle\sigma_{xy}^{(2)}\rangle$. Since the second mechanism does not contribute to first order, it is permissible to set $\pi^{\pm} = p^{\pm} = i\omega m(x \pm iy)$. The total weight $\langle\sigma_{xy}^{(2)}\rangle$ corresponding to a given interband transition becomes, from Eq. (3),

$$\langle\sigma_{xy}^{(2)}\rangle = \frac{\pi n e^2}{4\hbar} \sum_{\alpha\beta} \left[\omega_{\alpha\beta}\left|(x-iy)_{\alpha\beta}\right|^2 - \omega_{\alpha\beta}\left|(x+iy)_{\alpha\beta}\right|^2\right] . \qquad (24)$$

In the atomic model being considered, the contribution to $\langle\sigma_{xy}^{(2)}\rangle$ in the solid results from assuming that the total atomic oscillator strengths remain the same in the solid, and are only spread out in energy because of band effects. We assume, as suggested by the band-calculation results, that there is not appreciable mixing of upper atomic states or $4f$ states into the conduction band. With this assumption, the f-sum rule[29] states the total oscillator strength of transitions between p and d states will total the same for both the atomic model and the solid. In performing the atomic calculations, both atomic energies and wave functions must be used. The other assumption needed is that the band broadening does not change the difference in average energy introduced by spin-orbit coupling. This is also correct because band effects do not change the average energy: Calculating the trace of the Hamiltonian by using Bloch states or using atomic states gives the same result. From these arguments, we predict that the atomic calculation will give a good approximation of the weight $\langle\sigma_{xy}^{(2)}\rangle = \int\sigma_{xy}^{(2)}(\omega)d\omega$. Since the shape of $\sigma_{xy}^{(2)}(\omega)$ cannot be obtained from this approach, for this feature we must be guided by the results of band calculations.

In the spirit of the discussion just given, we use Eq. (24) to estimate the total weight for $f \rightarrow d$, $d \rightarrow f$, $d \rightarrow p$, and $p \rightarrow d$ transitions in the solid. Matrix elements for $x \pm iy$ are given by Bethe and Salpeter[30]; the overlap integrals for the $f \rightarrow d$ and $d \rightarrow p$ matrix elements were obtained by numerical integration of Herman and Skillman's atomic wave functions.[26] The results are

$$|R|_{pd}^2 = 2320(\mu^2 a_0)^2 \ , \quad |R|_{fd}^2 = 121(\mu^2 a_0)^2 \ , \qquad (25)$$

where $(\mu^2 a_0)^2 = 6.7\times10^{-20}$ cm^2, a_0 being the Bohr radius and μ being a scale factor given by $\mu = \frac{1}{2}(\frac{3}{4}\pi)^{2/3}(z)^{1/3} = 0.221$, where $z = 64$ is the atomic number of Gd. Spin-orbit splitting of d and f states is assumed equal to the atomic splittings as calculated by Herman and Skillman:

$\Delta E_{so} = 0.077 m_l$ eV, d states

$$\Delta E_{so} = 0.132 m_l \text{ eV}, \quad f \text{ states} \tag{26}$$

where m_l specifies the magnetic quantum number for particular states.

We now briefly outline the calculation of weights of $\sigma_{xy}^{(2)}(\omega)$ using the atomic picture just presented. Consider transitions from occupied states with p character to bands formed predominantly from Y_2^1 and Y_2^{-1} atomic d states, where the spherical harmonics Y_l^m represent the angular part of the wave function. Using the atomic picture, and calculating matrix elements of $x \pm iy$ for spin-up electrons, the contributions for Y_2^1 and Y_2^{-1} are found to be equal and opposite, giving rise to line strengths W as shown in Fig. 13(a). The weight W is the quantity related to the f-sum rule which by assumption remains constant in both the atom and solid in our model. In the solid, W can be associated with not only $d \rightarrow p$ transitions, but also $p \rightarrow d$ transitions. These two weights, W_{pd} and W_{dp}, we expect to have the same absolute magnitude since, in the atom, they are equal and opposite, corresponding to absorption and emission processes. In the solid, these weights must be multiplied by the parameters n_p and n_d, respectively, which specify the number of p- and d-character electrons. Band effects are assumed to broaden the lines but preserve the weight W, and spin-orbit coupling removes the degeneracy of the two levels, shifting them as shown in Fig. 13(b). Subtracting the two curves yields a quantity proportional to the spin-up contribution to $\langle\sigma_{xy}^{(2)}\rangle$ by transitions from p states to the $Y_2^{\pm 1}$ d bands. The result of this subtraction is shown in Fig. 13(c). Note that the weight W is reduced by the factor $(\Delta E_{so}/\Delta E_{\text{band}})$. Spin-down states produce an equal but opposite contribution which exactly cancels the effect of spin-up states when there is no net magnetization. To obtain $\langle\sigma_{xy}^{(2)}\rangle$ appropriate for the solid, we must also weight the appropriate oscillator strengths W by the spin-polarization of d states which accounts for exchange effects.

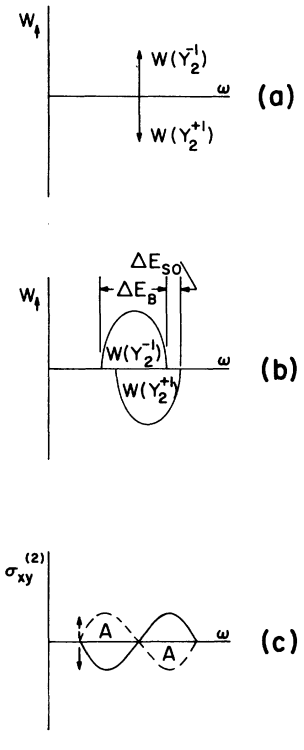

FIG. 13. Calculation of magneto-optic Kerr effects: (a) Oscillator strength $W_\uparrow$ for spin-up states resulting from $p \rightarrow d(Y_2^1)$ and $p \rightarrow d(Y_2^{-1})$ interband transitions. (b) Spin-orbit splitting ΔE_{so} and band broadening effects ΔE_B added to (a), weights preserved. (c) Substract the two curves to obtain net magneto-optic absorption for transitions between the spin-up states (solid line) corresponding contribution for spin-down states (dashed line). Note weight is reduced, $A = (\Delta E_{so}/E_B)W$, and that when $\tilde{M} = 0$ (equal population of spin-up and spin-down states), $\langle\sigma_{xy}^{(2)}\rangle = \langle\sigma_{xy\uparrow}^{(2)}\rangle + \langle\sigma_{xy\downarrow}^{(2)}\rangle = 0$.

Exchange effects are included using Stoner's picture of ferromagnetism. Figure 14(a) shows a representation of the density of states for the $Y_2^{\pm 1}$ states under discussion; one side corresponds to spin-up states the other to spin-down states. In an unmagnetized solid, the density of spin-up and spin-down states is the same. The Stoner picture accounts for ferromagnetism by assuming spin-up and spin-down states "see" a different effective field which is equivalent to shifting the curves relative to each other as shown in Fig. 14(b). The net spin density as a function of energy is proportional to the difference, and is shown in Fig. 15. Note each d band exhibits an inversion of spin density as a function of energy due to the shift. Referring back to Fig. 13 it is clear that the contributions to $\langle\sigma_{xy}^{(2)}\rangle$ resulting from this shift are additive; that is, at lower energies where spin-up electron densities are higher, $\langle\sigma_{xy}^{(2)}\rangle$ is shown negative; at higher energies, spin-down electron densities are higher, and these also yield a negative contribution. The net effect for $\langle\sigma_{xy}^{(2)}\rangle$ for transitions to Y_2^1 and Y_2^{-1} states are contributions of the same sign, and a total weight equal to $2W(\Delta E_{so}/\Delta E_{\text{band}})\langle\sigma\rangle$ is obtained. There are also similar contributions to the total $p \rightarrow d$ interband absorption produced by transitions to the $Y_2^{\pm 2}$ states. In the solid, we assume that all of the $Y_l^{\pm m}$ states are uniformly spread over the band. This assumption is valid, as is the case for Gd, as long as band-broadening effects dominate crystal-field effects which tend to split the d states into the appropriate crystal-field levels. After summing the weights of all $Y_l^{\pm m}$ connected by $x \pm iy$, the results are weighted by the occupation numbers of states involved, yielding the final result.

The computation for $f_\uparrow \rightarrow d_\uparrow$ and $d_\downarrow \rightarrow f_\downarrow$ weights is

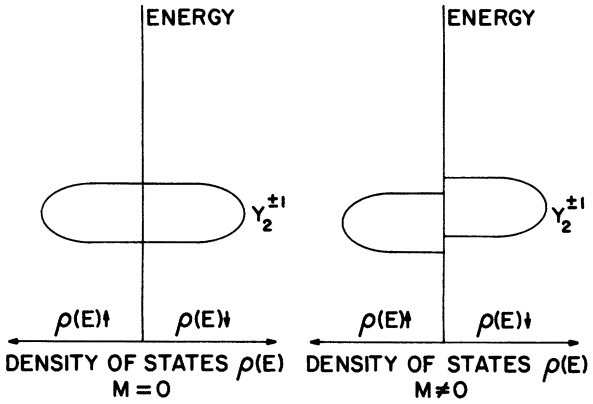

FIG. 14. Stoner band picture ferromagnetism, showing $Y_2^{\pm 1}$ contribution to the d-band spin-up and spin-down density of states $\rho(E)$ for both zero and nonzero magnetization $\vec{M}$.

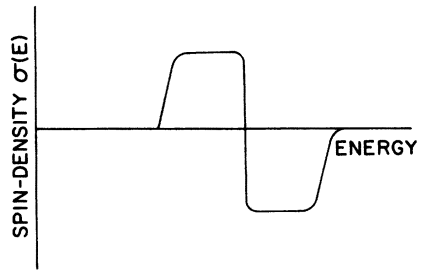

FIG. 15. Schematic representation of the net spin density expected from the Stoner model as a function of energy for a particular band when an exchange splitting exists.

slightly different since in these transitions, only majority and minority spin states are involved, respectively. Also, for $d \rightarrow p$ transitions there is no inversion of spin density since only the bottom of the d band is occupied. Therefore the factor of 2 for spin-up and spin-down states is not required, and the frequency dependence of the structure will be as shown in Fig. 13(c), the dotted line corresponding to $f_\uparrow \rightarrow d_\uparrow$ and the solid line corresponding to $d_\downarrow \rightarrow f_\downarrow$. The weights calculated in Table I for $f_\uparrow \rightarrow d_\uparrow$, $d \rightarrow p$, and $d_\downarrow \rightarrow f_\downarrow$ transitions correspond to the initial (low-energy) peak. The high-energy peak, which occurs above the low-energy peak at an energy of the order of the bandwidth, will be of opposite signs from the low-energy peak.

Table I lists the weights $\langle \sigma_{xy}^{(2)} \rangle$ corresponding to allowed magneto-optic transitions which were obtained as just outlined. Included in the table is a summary of various parameters used in the calculation. In the first row, we have equated the experimentally estimated weight of 3.6×10^{28} sec^{-2} resulting from $p \rightarrow d$ transitions to the calculated value in order to obtain $n_p = 6n_\alpha$, the effective number of p-character conduction electrons. The number is found to be 0.6 or approximately 20% of the total number of conduction electrons. The experimental estimate 3.6×10^{28} sec^{-2} is determined by subtracting the intraband term estimated by Eq. (22) from the experimental data of Fig. 5 and multiplying the remaining area by a factor of 1.8. Since the experimental data cover only part of the

TABLE I. Summary of parameters used in the model calculation. The various columns list information as follows: (i) interband transition; (ii) constants; (iii) energy difference $(\omega_\alpha - \omega_\beta)/\hbar$; (iv) and (v) sum of matrix elements including spin-orbit and band effects (see text); (vi) spin polarization; (vii) and (viii) the number of occupied and empty states; (ix) final result for the weight of magneto-optic absorption. The weights $\langle \sigma_{xy}^{(2)} \rangle$ should be regarded as order of magnitude estimates, which have been made in order to support interpretation of the data. The signs, however, are correct and very significant as discussed. Bar over n specifies occupied states. No bar over n specifies unoccupied states. Parentheses ( ) inside the table indicate final calculated values $|M|^2 \equiv \sum_{\alpha\beta}(|X_{\alpha\beta}^-|^2 - |X_{\alpha\beta}^+|^2)$.

Transition $\alpha \rightarrow \beta$	$\frac{\pi n e^2}{4h^2}$ (cm^{-2} sec^{-2}/eV)	$\Delta E \alpha\beta$ (eV)	$2\|M\|^2 \frac{\Delta E_{so}}{\Delta E}$ (cm^2)	$\|M\|^2 \frac{\Delta E_{so}}{\Delta E}$ (cm^2)	$\sigma_z = \frac{n_{\alpha\uparrow} n_{\beta\uparrow} - n_{\alpha\downarrow} n_{\beta\downarrow}}{n_{\alpha\uparrow} n_{\beta\uparrow} + n_{\alpha\downarrow} n_{\beta\downarrow}}$	n_α	n_β	$\langle \sigma_{xy} \rangle_{\alpha\beta}$ (sec^{-3})
$p \rightarrow d$	8.0×10^{45}	5	$+4.7 \times 10^{-17}$		0.28	(0.1)	0.8	3.6×10^{28}
$d \rightarrow p$	8.0×10^{45}	5		2.3×10^{-13}	0.28	0.2	0.30	$(1.6 \times 10^{27})^a$
$f_\uparrow \rightarrow d_\uparrow$	8.0×10^{45}	15		3.0×10^{-18}	1	1	0.37	$(1.3 \times 10^{29})^a$
$d_\downarrow \rightarrow f_\downarrow$	8.0×10^{45}	5		-3.0×10^{-18}	1	0.072	1	$-(8.5 \times 10^{27})^a$

ΔE_γ's, n_α, and n_β equivalents

Transition	n_α	n_β	ΔE_γ
$p \rightarrow d$	$\frac{1}{6}\bar{n}_p$	$\frac{1}{10}n_d$	1 eV
$d \rightarrow p$	$\frac{1}{10}\bar{n}_d$	$\frac{1}{6}n_p$	1 eV
$f_\uparrow \rightarrow d_\uparrow$	$\frac{1}{7}\bar{n}_{f\uparrow}$	$\frac{1}{10}n_{d\uparrow}$	1 eV
$d_\downarrow \rightarrow f_\downarrow$	$\frac{1}{10}\bar{n}_{d\downarrow}$	$\frac{1}{7}n_{f\downarrow}$	1 eV

[a]Weight and sign of low-energy peaks. High-energy peaks will occur with same weight but opposite sign.

energy range where $p \rightarrow d$ transitions are expected to occur, we estimate from the density-of-states histogram of Fig. 10 that the measured weight 2.0×10^{28} sec^{-2} should be multiplied by 1.8 to account for this.

In the second row, we have used $n_p = 1.8$ to describe the number of unoccupied p-character electrons in computing the weight $\langle \sigma_{xy}^{(2)} \rangle$ for $d \rightarrow p$ transitions and have assumed, as suggested by Fig. 11, that the sp band extends over 10 eV. The factor of 3 greater for the total of the unoccupied p-character states above E_F results from inspection of the density-of-states curve which shows that the number of unoccupied states is nine, three times the number of occupied states. Additional parameters used in the calculations of interband weights are as follows: $n = 0.305 \times 10^{23}$ cm^{-3}; $\langle \sigma \rangle_{4f} = 1$, indicating that the $4f$ electrons are assumed to be completely spin polarized; and $\langle \sigma \rangle_d = 0.28$, the same value used in the intraband computations. The s- and p-character conduction electrons are assumed to be unpolarized and unaffected by spin-orbit coupling. Therefore, in this model, $s \rightarrow p$ interband transitions do not contribute to magneto-optic effects. Note that the $d_\downarrow \rightarrow f_\downarrow$ transitions give a negative contribution in contrast to the other contributions.

The sum rule [Eq. (20)] was also evaluated using an atomic model. For Gd, the sum rule is primarily determined by the seven $4f$ electrons which are 100% spin polarized and which are tightly bound near the core where the matrix elements of the $\nabla^2 V(r)$ operator are large. Using Fig. 8 to estimate the charge distribution of $4f$ electrons, the sum rule is estimated to be

$$\int_0^\infty \omega \sigma_{xy}^{(2)}(\omega)\, d\omega \cong -8 \times 10^{44} \text{ sec}^{-3}. \tag{27}$$

In deriving Eq. (20) it was assumed that $e > 0$ so that the charge on an electron is $-e$. The sum rule universally gives a negative result when the positive direction is chosen as the majority spin direction, as is the convention in this paper. In the energy range covered by our experimental data, the total weight is approximately equal to $+7 \times 10^{44}$, most of this weight resulting from the intraband component. It is clear that a large negative contribution is needed to satisfy the sum rule. Part of this contribution will come from the $f_\uparrow \rightarrow d_\uparrow$ transitions which from Table I are seen to contribute a weight of -2×10^{44} sec^{-3} to the sum rule. In order to exhaust the sum rule, $f_\uparrow \rightarrow g_\uparrow$ transitions must also be considered. We expect from our model that $f_\uparrow \rightarrow g_\uparrow$ transitions will give a negative contribution and it is not unreasonable that it will have sufficient strength to complete the sum rule.

VII. DISCUSSION

The estimated intraband contribution to $\sigma_{xy}^{(2)}(\omega)$ given by Eq. (22) accounts for the main ω^{-1} trend in the background in the experimental data shown in Figs. 5 and 12. The magnitude of conduction-band–d-state–wave-function spatial polarization, $|P_0'|$, used to obtain this result is consistent with spin-orbit energies which are the driving mechanism. The other parameters used in obtaining Eq. (22), i.e., the carrier lifetime and spin polarization, were inferred from independent experimental results. Subtracting this term from experimental data leaves the interband contribution consisting of two peaks and some background with a total weight 2.0×10^{28} sec^{-2}, as shown in Fig. 5.

This structure we interpret as resulting from interband transitions from occupied states of p character near the Fermi level to d states above the Fermi level. The band-structure calculations for Gd support this viewpoint, and we have demonstrated that the magnitude of these peaks can be understood from computations based on a simple model. These calculations suggest that the p character of the occupied conduction-band states is approximately 20% of the total occupied states. This value may be in error as much as a factor of 3, and reflects the limitations of the simple approach used in the calculations.

It is interesting to note that the transition-metal ferromagnets exhibit conduction-band properties which are very similar to what we have observed in Gd. The magneto-optic behaviors of Fe, Ni, and Co all exhibit the characteristic double peak in $\sigma_{xy}^{(2)}(\omega)$, in the 1–5 eV energy range,[31] and tight-binding calculations[24] for d bands of these metals exhibit d-band splitting similar to that shown in Fig. 10. In the ferromagnetic transition metals, the d bands are primarily below the Fermi level, and the appropriate interband transitions are predominantly $d \rightarrow p$. Justification for this interpretation is much the same as we have argued for Gd although we have backed our interpretation in the case of Gd by some numerical estimates.

There is one more interesting feature of $\sigma_{xy}^{(2)}(\omega)$ which we now discuss. This feature is the rapid decrease and change of sign of the interband part of $\sigma_{xy}^{(2)}(\omega)$ starting at about 4.5 eV. This is not due to $d \rightarrow p$ transitions since this contribution is too weak or $p \rightarrow d$ transitions since the sign is wrong, and intraband effects clearly cannot cause the behavior. Herbst, Lowy, and Watson[28] have recently calculated the relative position of ground-state $4f$ configurations relative to the d bands and Fermi level in rare-earth metals and also the position of the excited $4f$ level above E_f. Their results, shown in Fig. 16, predict unoccupied $4f$ levels at about 3.6 eV above E_f in Gd and at about 2.2 eV in Dy. We interpret the abrupt change in $\sigma_{xy}^{(2)}(\omega)$ for Gd as resulting from $d_\downarrow \rightarrow f_\downarrow$ transitions. The results of Table I show that this transition will contribute a weight to $\sigma_{xy}^{(2)}(\omega)$ of opposite sign to $d \rightarrow p$

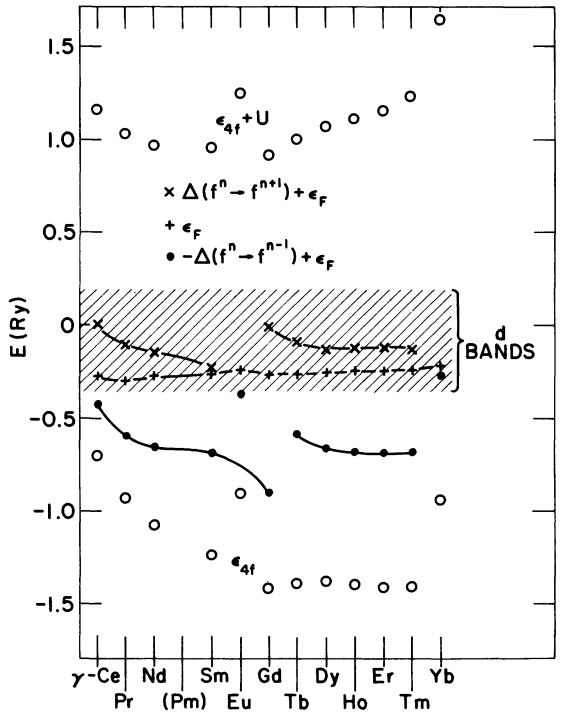

FIG. 16. Calculated levels of filled $4f$ states (circles), d bands (cross-hatched area), Fermi level (+), and excited states for f^{n-1} (●) and f^{n+1} (×) configurations [Herbst *et al.* (Ref. 28)].

and $p \rightarrow d$ transitions. The threshold for $d_\downarrow \rightarrow f_\downarrow$ transitions based on our data is therefore about 4.6 eV. We have carried out a preliminary investigation of magneto-optic effects in dysprosium metal, and the results are also in general agreement with the theoretical results of Herbst *et al.* The low-energy (< 2.5 eV) magneto-optic behavior of dysprosium is similar to that of gadolinium. Above 2.5 eV, $\sigma_{xy}^{(2)}(\omega)$ for dysprosium exhibits a large-amplitude negative peak, with a total weight $\langle\sigma_{xy}^{(2)}\rangle$ which is very close to what our calculations predict for transitions from occupied $4f_\downarrow$ states to d states above the Fermi level. This observation gives us confidence in our calculations and the interpretation of our data. The results for dysprosium will be published in a separate paper.

The fact that the magneto-optic absorption $\sigma_{xy}^{(2)}$ can be either positive or negative is an important feature which represents one advantage of this technique over ordinary optical experiments. In the present case, the sign has been crucial in allowing us to identify the effects of minority-spin transitions to unfilled $4f$ states exhibited by experimental data. It is also interesting to note that the sum rule, Eq. (28), requires negative contributions to balance the positive contribution observed in the 1–5-eV range. The $d_\downarrow \rightarrow 4f_\downarrow$ transitions will provide some of this negative contribution.

In Fig. 12, the function $\omega\sigma_{xy}^{(2)}$ corresponding to experimental data has been plotted. As shown by Eq. (6), the interband part of $\omega\sigma_{xy}^{(2)}$ is roughly proportional to the joint density of states assuming the oscillator strengths are approximately constant. In Gd this joint density of states is roughly proportional to the unoccupied d-band density of states as justified in the next paragraph. The portion of area above the dotted line in Fig. 12 therefore respresents the unoccupied d-band density of states and is also plotted on Fig. 10 for comparison with calculated values. Some of the high-energy part of the d-band contribution to $\omega\sigma_{xy}^{(2)}$ as shown by Fig. 12 may be obscured by the $d_\downarrow \rightarrow f_\downarrow$ threshold which would tend to partially cancel the $p \rightarrow d$ contribution above the $d_\downarrow \rightarrow f_\downarrow$ threshold. We note that the structure in the experimental curve is sharper than the calculated values and that the position of the peaks matches that of the calculation only qualitatively.

The crucial assumptions to interpret $\omega\sigma_{xy}^{(2)}$ as the density of states of the unoccupied d bands in Gd are that (a) the occupied p states have a spread in energy small compared to the unoccupied d bandwidth, and (b) the factor $\overline{F}_{\alpha\beta}(\omega)$ in Eq. (6) is approximately constant. The sharpness of the peaks observed in the experimental data, Figs. 5 and 12, prove that the p character of occupied states does not extend beyond an energy range of 1 eV, the width of the peaks. If it did, then the observed peaks widths would have been larger. Then the p character of the occupied states must be less than 1 eV, small compared to the unoccupied d bandwidth. Band calculations indicate that the bottom of the conduction band has pure s symmetry so that it is likely that the p character is concentrated near the Fermi level.

The approximate constancy of $F_{\alpha\beta}(\omega)$ follows from the model-calculation discussion of Sec. VI, where for a given type of transition, say $p \rightarrow d$, $F_{\alpha\beta}(\omega)$ is approximately constant. Only above about 4.5 eV, where $d_\downarrow \rightarrow f_\downarrow$ transitions start contributing, does $F_{\alpha\beta}(\omega)$ change. In fact, it has a change in sign besides a change in magnitude, and we have some uncertainty about the shape of the d band in this region. This uncertainty introduces the > sign in the experimental values of the unoccupied and total d bandwidths in Table II.

Table II summarizes band parameters predicted by our results. Figure 16 suggests the lower limit on unoccupied d bandwidth is 4.5 eV. If the spectra of $\sigma_{xy}^{(2)}$ were continued beyond 5 eV, the half-width of occupied d bands would be obtained as the width of the negative peak from $d_\downarrow \rightarrow f_\downarrow$ transitions which begin at 4.6 eV. The $4f_\downarrow$ states are placed 4.6 eV above the Fermi level as just discussed. Other experimentally determined parameters of the d band are also summarized in Table II.

TABLE II. Summary of band-structure details of Gd as determined experimentally and as calculated theoretically.

	This expt. (eV)	Herbst *et al.* (eV)	Dimmock *et al.* (eV)
Energy of unfilled $4f_{\downarrow}$ levels above E_F	4.6	3.6	...
Unoccupied d bandwidth	1	1.2	2
Total d bandwidth	≥ 5.5	7.0	8.0
Spacing between major peaks of unoccupied d bands	2.2	...	3
Peak positions above E_F	2.0	...	1.2
	4.0	...	4.2

VIII. CONCLUSIONS

In this paper, the first detailed study of magneto-optic effects in gadolinium metal has been presented. Our interpretation of the experimental results is in reasonable qualitative agreement with band calculations,[1] with the theoretical estimates of the position of excited $4f$ states in rare-earth metals, and with the location of the Fermi level,[28] though quantitative differences exist. We have estimated a number of parameters from our experimental data summarized in Table II, which include the d band properties, location of unoccupied $4f$ levels above the Fermi level, and, in addition, the amount of p character of occupied conduction-band electrons.

A phenomenological theory of intraband magneto-optic Kerr effects was presented and used to account for the "conduction-electron" contribution to experimental data. The expression for intraband magneto-optic effects predicts a frequency dependence and amplitude which agree with experimental data. The required value of conduction-electron spatial polarization denoted by P_0', a parameter in the theory, is consistent with the spin-orbit coupling strength of d-conduction electrons in the solid. An atomic model calculation modified to account for band effects was used to estimate total strength of various interband transitions in the solid. This approach was justified, and provided estimates which support the interpretations given to structure in magneto-optic data. The estimate of total weights for $4f \rightarrow 5d$ transitions indicates that these should be readily observable using magneto-optic techniques, whereas they have not been observed in ordinary optical experiments. The reason why magneto-optic techniques emphasize the role of the d and f states compared to ordinary optical techniques is that the magneto-optic absorptions are proportional to the product of the spin-orbit interaction and the net spin polarization. The d and f states probe the core potential much more strongly than do the conduction s and p states and thus have a substantially stronger spin-orbit interaction and spin-polarization. In fact our estimate is that $s \rightarrow p$ transitions are negligible for the magneto-optic effects in Gd. The ordinary optical absorptions are dominated by $s \rightarrow p$ transitions because their dipole matrix elements are so large, overwhelming any structure from d and f states.

It has been shown in this paper that magneto-optic measurements are a powerful technique in determining the electronic band structure of magnetic metals. Such measurements will provide an independent and more accurate check of the location of occupied $4f$ levels in the ferromagnetic rare-earth metals. A careful study of $4f \rightarrow d$-band transitions would also serve as a check on the shape of d bands established on the basis of $p \rightarrow d$-band magneto-optic absorption. There are many other future experiments suggested by the present results. The fact that semiquantitative estimates can be made using simple models provides motivation for studying the other magnetic rare-earth metals. The case of dysprosim is especially interesting as indicated by some preliminary results discussed briefly in this paper. Magneto-optic effects in Fe, Ni, and Co have been studied experimentally, but experimental results have not been used to full advantage in understanding the complicated nature of their d bands.

In addition to the main features of the band structure which we have focussed on in this paper, fine structure in magneto-optic data, especially when related to polarization or crystal orientation effects, should provide a powerful tool for checking details of band structures as more accurate and detailed calculations become available. High resolution is required to measure magneto-optic fine structure; however, the fine-structure features shown in Fig. 6 are genuine, as were verified by repeated measurements on the same sample at different temperatures. Continued improvements in experimental techniques will enable more comprehensive studies of magneto-optic fine structure to be made, and should result in the full development

of another valuable and powerful experimental technique for studying the properties of magnetic solids.

ACKNOWLEDGMENT

One of us (E.A.S.) would like to acknowledge very useful conversations with Professor A. J. Freeman.

---

*Based in part on research performed in partial fulfillment of the requirements for a Ph.D. degree at the University of Washington. Research supported in part by the Air Force Office of Scientific Research under AFOSR Grant No. AFOSR-71-1967.

[1]O. J. Dimmock, A. J. Freeman, and R. E. Watson, in *Optical Properties and Electronic Structure of Metals and Alloys* edited by F. Abeles (North-Holland, Amsterdam, 1966), p. 237. There have been several band calculations subsequent to this paper: A. J. Freeman, J. O. Dimmock, R. E. Watson, in *Quantum Theory of Atoms, Molecules and the Solid State, a Tribute to John C. Slater*, edited by P. O. Lowdin (Academic, New York, 1966), p. 361; S. C. Keeton and T. L. Loucks, Phys. Rev. **146,** 429 (1966); S. C. Keeton, and T. L. Loucks, Phys. Rev. **168,** 672 (1963); G. S. Fleming, S. H. Lik, and T. L. Loucks, Phys. Rev. Lett. **21,** 1524 (1968); O. K. Anderson and T. L. Loucks, Phys. Rev. **167,** 551 (1968).

[2]J. G. Endriz and W. E. Spicer, Phys. Rev. B **2,** 6 (1970).

[3]A. J. Blodgett, Jr., W. E. Spicer, and A. Y-C. Yu, Ref. 1, p. 246; C. Cr. Schüler, Ref. 1, p. 221.

[4]G. Brodin, S. B. M. Hagström, and C. Norris, Phys. Rev. Lett. **24,** 1173 (1970); P. O. Heden, H. Löfgren, and S. B. M. Hagström, Phys. Rev. Lett. **26,** 432 (1971); G. Busch, M. Campagna, P. Cotti, and H. Ch. Siegmann, Phys. Rev. Lett. **22,** 597 (1969); G. Busch, M. Campagna, D. Pierce, and H. Siegmann, Phys. Rev. Lett. **28,** 611 (1972).

[5]S. B. A. Politzer and P. H. Cutler, Phys. Rev. Lett. **28,** 1330 (1972).

[6]B. R. Cooper, Phys. Rev. **139,** A1504 (1965).

[7]H. S. Bennett and E. A. Stern, Phys. Rev. **137,** A448 (1965).

[8]H. R. Hulme, Proc. R. Soc. Lond. **135,** 237 (1932).

[9]The states $|\alpha\uparrow\rangle$ are not eigenstates because of spin-orbit coupling, but just the spin-up component of an eigenstate.

[10]R. Karplus and J. Luttinger, Phys. Rev. **95,** 1154 (1954).

[11]J. Smit, Physica (Utr.) **21,** 827 (1955).

[12]R. C. Fivaz, Phys. Rev. **183,** 586 (1969).

[13]L. Berger, Phys. Rev. B **2,** 1459 (1970).

[14]E. A. Stern, Phys. Rev. Lett. **15,** 62 (1965); J. L. Erskine and E. A. Stern, J. Appl. Phys. **41,** 1246 (1970).

[15]This method is discussed in detail by A. B. Pippard [Rep. Prog. Phys. **23,** 176 (1960)] and is equivalent to a formal solution of Boltzmann's equation.

[16]S. Doniach, Ref. 1, p. 471.

[17]Similar instruments have been discussed in detail previously, see, for example, Surf. Sci. **16,** 177 (1969); **16,** 288 (1969).

[18]J. C. McGroddy, A. J. McAlister, and E. A. Stern, Phys. Rev. **139,** A1844 (1965).

[19]J. L. Erskine, Doctoral thesis (University of Washington, 1972) (unpublished).

[20]M. J. Frieser, IEEE Trans. Magn. **4,** 152 (1968).

[21]J. N. Hodgson, J. Phys. C **2,** 97 (1968); and private communication.

[22]C. J. Flaten (private communication).

[23]Some speculations are made in Ref. 19 concerning the origin of some observed structure, based on band-structure calculations of Dimmock *et al.* and selection rules for allowed transitions.

[24]S. Wakoh and J. Yamashita, J. Phys. Soc. Jap. **21,** 1712 (1966); E. F. Belding, Philos. Mag. **4,** 1445 (1959); G. C. Fletcher and E. P. Wohlforth, Phys. Met. Metallogr. **42,** 106 (1951).

[25]J. Friedel, in *The Physics of Metals*, edited by J. M. Ziman (Cambridge U. P., Cambridge, England, 1969), Chap. 8.

[26]F. Herman and S. Skillman, *Atomic Structure Calculation* (Prentice-Hall, Englewood Cliffs, N. J. 1965).

[27]P. O. Heden, H. Lofgren, and S. B. M. Hagström, Phys. Status Solidi B **49,** 721 (1972).

[28]J. F. Herbst, D. N. Lowy, and R. E. Watson, Phys. Rev. B **6,** 1913 (1972).

[29]A. H. Wilson, *The Theory of Metals* (Cambridge U. P., Cambridge, England, 1953), p. 47.

[30]H. Bethe and E. Salpeter, *Quantum Mechanics of One- and Two-Electron Atoms* (Springer-Verlag, New York, 1957).

[31]G. S. Krinchik and B. A. Artemjev, J. Appl. Phys. **39,** 1276 (1968).